A stably-stratified atmospheric inflow assimilated to measured mean profiles interacting with a wind park

Journal of Physics: Conference Series **2767** (2024) 052054 doi:10.1088/1742-6596/2767/5/052054

A stably-stratified atmospheric inflow assimilated to measured mean profiles interacting with a wind park

Linus Wrba[1], Lukas Bührend[1], Antonia Englberger[1], Andreas Dörnbrack[1] and Norman Wildmann[1]

[1]Deutsches Zentrum für Luft- und Raumfahrt, Institut für Physik der Atmosphäre, Oberpfaffenhofen, Germany

E-mail: linus.wrba@dlr.de

Abstract. In this paper, a simulation chain is presented. This method comprises the precursor large-eddy simulation (LES) of a stably-stratified atmospheric boundary layer (ABL), the assimilation of the simulated mean velocities to measured wind profiles, and finally a simulation of the generated turbulent ABL flow passing through two wind turbines in a row. The high-resolved precursor simulation with a horizontal grid spacing of 3 m accounts for the characteristic turbulence of the stably-stratified ABL. Using an assimilation technique, the horizontal velocities are adapted accurately to the measured mean wind profiles for the WiValdi wind farm site at Krummendeich. The wakes of two wind turbines in a row with the assimilated inflow is successfully computed. With the simulation chain presented, it is possible to generate realistic atmospheric inflows for wind-turbine simulations with manageable computational effort.

1. Introduction

The vertical distributions of wind, temperature, moisture, and turbulence in the ABL strongly depend on the diurnal cycle. During day, the solar heating of the surface generates turbulent up- and downdraughts, resulting in a well-mixed ABL. After sunset, the surface cooling produces negative buoyancy and leads to a sink in turbulence production. During this period, the main turbulence production mechanism is mechanical shear close to the surface. There are also other turbulence sources like breaking gravity waves or advection of turbulence during night, all together describing nocturnal intermittent turbulence [1].

To realistically generate turbulence locally and preserve it in a stably-stratified ABL with an LES model, a very fine spatial resolution of less than about 3.125 m is required [2]. In addition, an appropriate subgrid-scale (SGS) model must represent the unresolved turbulence [3]. For stably-stratified flows, the SGS model has to account for buoyancy destruction in the vertical [4] as well as for the anisotropy of turbulence [5]. Considering these requirements, the stably-stratified ABL flow can be simulated numerically by idealized LES models [3, 6, 7].

A realistic wind-park inflow is characterized by variable, mostly transient 3 D wind and temperature fields. In numerical models, they can be separated into mean vertical profiles of the three wind components and the temperature and their corresponding turbulent fluctuations. The application in wind energy often requires that these mean vertical profiles used as initial and background states in LESs are as close as possible to measured or simulated nocturnal profiles (e.g. from mesoscale models) in order to represent specific cases. Various approaches exist to include this meso-microscale coupling in LESs [8, 9]. The general idea is to apply a nudging

of mean profiles from a precursor simulation towards a new target profile of the horizontal wind. It is crucial for the assimilation technique to avoid a damping effect on the characteristic atmospheric turbulence from the precursor simulation.

The final goal would be a highly-resolved wind-park simulation with realistic mean profiles as well as turbulence fields. However, this is especially difficult in case of intermittent flow simulations [10]. Therefore, this work presents an intermediate step towards the final goal of not only adapting the mean profile towards a specific target profile, but also letting the turbulence develop adequately under the influence of the new profile.

The paper is organized as follows: The atmospheric situation, the numerical model EULAG, the precursor simulation of the stable boundary layer (SBL), the data assimilation technique, the wind-farm simulation, and the coupling strategies required to combine the three individual components of the simulation chain are described in Sect. 2. The respective numerical results follow in Sect. 3, with a detailed view on wind-turbine relevant heights. Conclusions are given in Sect. 4.

2. Methodology

Measurements of the horizontal wind at the Krummendeich site (cf. Section 2.1) are applied as reference for our simulations. All numerical simulations are conducted with the numerical solver EULAG, whose properties and settings are briefly described in Section 2.2.

Following literature, we apply a simulation chain, consisting of three components (see Figure 1): the precursor simulation described in Section 2.3 is used to establish a first approximation to wind measurements of an SBL. Further, this simulation ensures an appropriate vertical profile of the potential temperature of the subsequent simulations. The numerical simulation results serve as input for the relaxation method discussed in section 2.4, where a forcing is applied to nudge the zonal and meridional velocity components towards the measured wind components. Finally, the atmospheric flow fields of the precursor simulation as well as the assimilation simulation were applied as inflow field in the wind-farm simulations. The setup of the wind-farm simulations are described in section 2.5.

2.1. The atmospheric situation

The references for the simulation chain are horizontally averaged vertical profiles of potential temperature and horizontal wind components. These quantities were measured by a microwave radiometer and a Doppler wind lidar [11] at the Krummendeich research windpark WiValdi [13] on 18 November 2021 at 03:35 UTC (Figs. 2 and 3, gray dotted lines). The lidar data are available down to a height of 60 m. The zonal (u) and meridional (v) wind components below that height were approximated by linear extrapolation from the measured values at 60 m, because this data is necessary for the data assimilation method explained in Section 2.4. This extrapolation is not necessary for the turbulent kinetic energy (TKE) data. The main characteristics of an SBL are present in these measurements: A low-level jet (LLJ) between the height of 300 m and 400 m and a temperature inversion in the temperature profile. The specific TKE ($= \frac{1}{2}[u'^2 + v'^2 + w'^2]$, primes denote deviations from the horizontal mean) obtained from the measurements shows an increase below 400 m and a constant intensity of $\approx 0.2\ \frac{\mathrm{m}^2}{\mathrm{s}^2}$ between 400 m and 800 m altitude. The variance of the flow is considered by including an uncertainty region to the measurements (gray shaded area in Figs. 2 and 3) which is ± 0.5 m s^{-1} for the velocity and 0.2 m^2 s^{-2} for TKE following Wildmann et al. [11].

2.2. The numerical model EULAG

EULAG is a multiscale geophysical flow solver, which integrates the three-dimensional incompressible Boussinesq equations for the resolved zonal, meridional and vertical wind components u, v, w and the resolved potential temperature perturbation θ' [12]:

$$\boldsymbol{\nabla} \cdot (\rho_0 \mathbf{v}) = 0, \tag{1}$$

$$\frac{\mathrm{d}\mathbf{v}}{\mathrm{d}t} = -\boldsymbol{\nabla}\left(\frac{p'}{\rho_0}\right) + \mathbf{g}\frac{\theta'}{\theta_0} - \mathbf{f}_c \times (\mathbf{v} - \mathbf{v}_e) - \boldsymbol{\nabla} \cdot \tau - \mathbf{f} + \frac{\mathbf{F}_{WT}}{\rho_0}, \tag{2}$$

$$\frac{\mathrm{d}\theta'}{\mathrm{d}t} = -\mathbf{v} \cdot \nabla\theta_e - \boldsymbol{\nabla} \cdot \vartheta. \tag{3}$$

Here, the environment state is denoted with the subscript e. Further, $\mathbf{v} = (u, v, w)$, p is the pressure, $\rho_0 = 1.1$ kg m^{-3} a constant density of the dry atmosphere, $\mathbf{g}$ the gravity vector and $\mathbf{f}_c = (0, 0, 2\Omega_c \sin\phi)$ is the Coriolis frequency with Ω_c the angular velocity vector resulting from the rotation of the Earth and $\phi = 53.9°$ the latitude of Krummendeich. The dissipation of momentum and heat is prescribed with the divergence of the SGS stress τ and flux ϑ, respectively. $\mathbf{f}$ denotes the additional forcing due to the assimilation method described in Sect. 2.4. The turbine-induced forces are implemented via the immersed boundary method modifying the flow field via $\mathbf{F}_{WT}$, prescribing the forces as actuator disc method following the blade-element momentum theory.

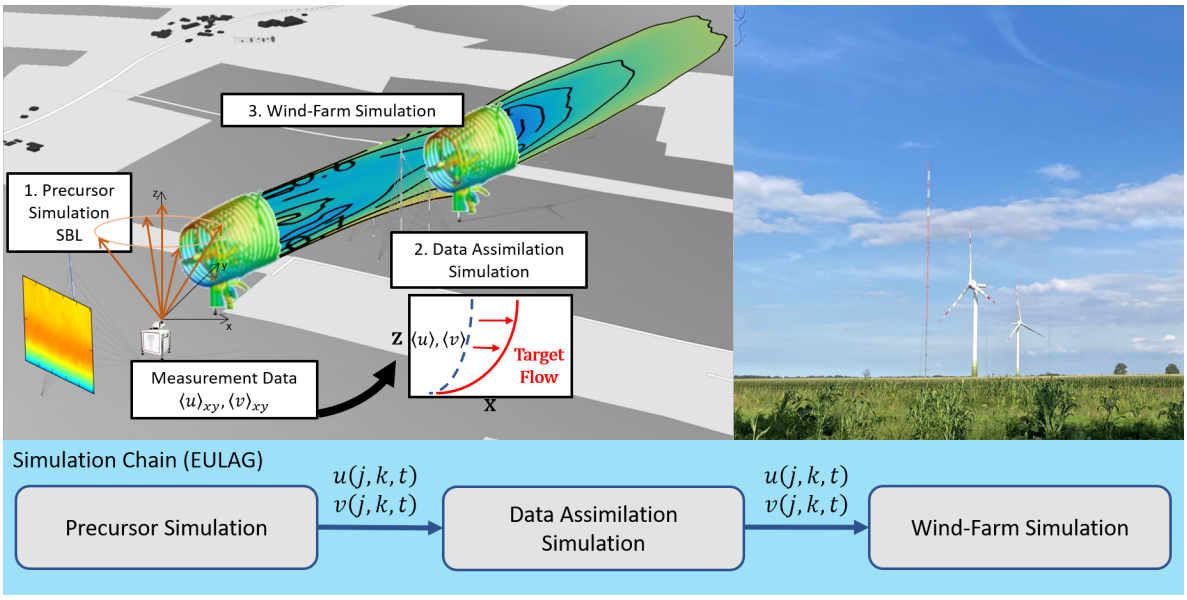

Figure 1. Schematic visualization of the simulation chain on the left and bottom and picture of the two wind turbines at Krummendeich (15.08.2023) on the right. The 2D-slices of the idealized precursor simulation profiles (1.) are used as input for the data assimilation technique (2.) which nudges the zonal and meridional wind velocity components u and v towards the horizontal averaged target profiles measured at Krummendeich. 2D-slices from this simulations serve as the inflow conditions for the subsequent wind-farm simulation (3.), where the performance of two wind turbines in the stable boundary layer is tested. All simulations are conducted with the numerical solver EULAG.

In this paper, EULAG is used with the TKE SGS model according to Schumann [4] to close the governing equations. A partial slip Neumann boundary condition with surface fluxes for momentum is applied at the lower boundary for the horizontal wind components. A heat flux of $-10\times10^{-3}\,\frac{\mathrm{K\,m}}{\mathrm{s}}$ is imposed on the lower boundary, resulting in a total surface cooling of $-0.4\,\mathrm{K}$ in the 9 simulated hours. A sponge layer was imposed on the upper boundary to dampen numerical oscillations.

In the horizontal directions, periodic boundary conditions are used for all prognostic variables. For all simulations, the horizontal grid sizes are $\Delta x = \Delta y = 3$ m, which is chosen to be below the limit suggested by Maronga and Li [2]. Vertical stretching is applied with $\Delta z_{min} = 2.2$ m at the lower boundary, $\Delta z_{max} = 15.5$ m at the upper boundary and a continuous increase in between. This grid refinement ensures a fine resolution close to the surface and in the typical vertical domain of wind turbines while maintaining a reasonable fast computation time. For the top cells, a resolution in z direction as fine as for the bottom cells is not necessary in this idealized SBL simulation, since turbulence occurs mainly below z $\approx$ 500 m and velocity profiles become uniform above the low level jet.

2.3. Precursor simulation of an SBL

The simulated domain spans 600 m $\times$ 600 m $\times$ 800 m in x, y and z directions with 200 gridpoints in the horizontal and 160 in the vertical directions. An anisotropy model following Sullivan et al. [5] is implemented and modifies the SGS stress tensor τ_{ij} to take into account the reduction of turbulence length scales and the inhomogeneous flow close to the surface and to obtain resolved turbulence.

The initial and background environmental vertical profile of the potential temperature is

$$\theta_e(z) = \begin{cases} 280\ \mathrm{K} & z \leq 100\ \mathrm{m} \\ 280\ \mathrm{K} + 0.01\ \mathrm{K/m} \cdot (z - 100\ \mathrm{m}) & z > 100\ \mathrm{m} \end{cases} \tag{4}$$

The initial and background horizontal wind components are $u(z) = 15\,\frac{\mathrm{m}}{\mathrm{s}}$ and $v(z) = -3\,\frac{\mathrm{m}}{\mathrm{s}}$. Within the simulated time period of 9 h, a quasi-steady state is reached, meaning that the mean vertical profiles of u and v barely change with time.

2.4. Data assimilation

Several meteorological mesoscale processes influencing the microscale flow cannot be represented sufficiently in LESs. The lack of adequate representation of these processes limits the possibility of carrying out LES with previously defined settings in order to match observed flow parameters [10]. Using data assimilation techniques, an additional forcing can be applied to the zonal and meridional velocity components in order to nudge the simulated velocities towards the observed target values. Various approaches for data assimilation methods can be found in literature which are used both in mesoscale models like the weather research and forecasting model (WRF) [17] and microscale models [16]. However, there are unresolved issues concerning the damping of the resolved atmospheric turbulence by these assimilation techniques. Here, we implement and apply a method developed by Nakyama and Takemi [9] which is based on the vibration equation for the velocity oscillating around a zero-wind basic state with a certain frequency. The following forcing term $\mathbf{f}$ is derived from the vibration equation and is introduced on the right hand side of the momentum equations in Eq. 3:

$$\mathbf{f}(x,y,z,t) = \rho_0 \omega_0^2 \int_0^t \left(\psi(x,y,z,t') - \Psi_{OBS}(z,t')\right)\,\mathrm{d}t' \quad . \tag{5}$$

ψ and Ψ_{OBS} correspond to the instantaneous horizontal velocity components u and v at a certain grid point and the averaged observed velocity components $U_{OBS}(z)$ and $V_{OBS}(z)$ at the related

height z, respectively. ρ_0 is the density and $\omega_0 = 2\pi f_0$ the frequency for the oscillating velocity in the vibration equation. This approach has successfully been applied for a near-neutral case of WiValdi in Wrba et al. [18].

In the nudged simulation, two-dimensional slices of the evolving velocity components and the potential temperature from the precursor simulation are used as synchronized inflow conditions at every time step. The dimensions of the nudging simulation are $3000 \times 600 \times 800$ m^3 with the same spacing as in the precursor simulation. The forcing due to the assimilation method is applied at every grid point i, j, k for $i = 60 \ldots 400$ ($x = 180 \ldots 1200$ m). The analysis section for the investigation of the assimilated profiles is from $x = 1200$ m to 1800 m.

2.5. Wind-farm simulation

To represent the arrangement of wind turbines inside the WiValdi wind farm, two wind-turbine rotors, one in the wake of the other, are implemented in EULAG. The domain size and spatial resolution is the same as in the data assimilation simulation. As wind turbine we apply the 5 MW NREL rotor with D = 126 m rotor diameter and 90 m hub height. These values are similar to both turbines of WiValdi which have a rotor diameter of 116 m and a hub height of 92 m. Due to similar dimensions, we choose this rotor as no data of the actual rotors are available. However, this is suitable for this investigation, as there are no wake measurements for comparison because the wind turbines were not yet finished in 2021 (time of atmospheric measurements). Comparable to WiValdi with a turbine distance of 508 m, we applied a turbine spacing of 504 m, corresponding to a turbine spacing of 4 D for the NREL 5 MW rotor.

2.6. Coupling strategies

As first step, the precursor simulation of the SBL is conducted with the initial and boundary conditions described in 2.3. After reaching a quasi-steady state, 2 D slices of the three velocity components and the potential temperature perturbation spanning the y - z-area are stored at every time step over a period of 20 min. They serve as input for the following assimilation simulation preserving turbulence with open horizontal boundary conditions.

The same procedure is repeated in the nudging simulation at $x = 1500$ m. The corresponding 2D slices are again used as turbulence recycling method for the input in the wind-turbine simulations. For a more detailed explanation we refer to Englberger & Dörnbrack [19].

3. Results

3.1. Precursor simulation

The resulting vertical profiles of horizontal wind and TKE (resolved + subgrid scale) from the idealized precursor simulation are obtained at the last time step by horizontal averages at each vertical level (Fig. 2). The LLJ height of the simulation, visible in the $\langle u \rangle_{xy}$-profile is between 300 m and 400 m, similar to the measurement. The mean zonal wind $\langle u \rangle_{xy}$ is larger in the simulation than in the measurement, especially close to the surface. The mean meridonal wind $\langle v \rangle_{xy}$ has smaller deviations from the observed profile with an overshoot above 300 m and small underrepresentation below. The simulated mean TKE is smaller compared to the values obtained at Krummendeich.

The differences of the mean profiles between the idealized precursor simulation and the experimental measurements can be explained as following. Multiple properties of the final wind and temperature profiles as well as the TKE and the boundary-layer height in the idealized simulations are correlated. A larger TKE could be obtained by increasing the surface heat flux, resulting in a larger surface temperature at the end of the simulation time. However, this would increase the height of the boundary layer and thus also the height of the LLJ (a detailed example of the correlation between boundary-layer height and surface cooling rate can be found in Sullivan [7]). But the height of the LLJ in the precursor simulation is already greater than in

the observations, and an increase in the surface heatflux would further amplify this difference. Another reason for the difference of simulated to measured profiles is the presence of mesoscale meteorological processes, which could be included by adding additional forcing terms in the equations. This is not taken into account in the idealized precursor simulation.

In summary, the mean vertical profiles obtained by the precursor simulation show differences to the measurements. This result is not unexpected and it is assumed that the data assimilation method as applied in the next step of the simulation chain will provide a framework for a realistic wind-park inflow.

3.2. Data assimilation

Figure 2 shows that despite a careful adjustment of all parameters in the precursor simulation there is still a difference between the vertical profiles in the LES and the measured profiles, which may result from mesoscale processes that are not represented in idealised LESs. With the data-assimilation technique described in Sect. 2.4, the zonal and meridional velocity components are nudged towards the observed target profiles. As a larger frequency f_0 in Eq. 5 leads to a stronger forcing, we expect a higher impact on the TKE as well. We tested the method for different frequencies f_0 to see its influence on the velocities and the TKE. The results for the simulation with data assimilation for different frequencies f_0 are shown in Fig. 2. The uncertainties of the variance of the flow in the measurements are indicated by the gray colored areas according to Wildmann [20].

A clear impact of the vibration assimilation method is evident from the profiles of the mean zonal velocity $\langle u \rangle_{xy}$ (averaged over $x = 1200$ m ... 1800 m) in the left image of Fig. 2: For a higher frequency f_0 the change of the velocity is larger compared to a smaller frequency. For $f_0 = 0.001$ s^{-1} and $f_0 = 0.0015$ s^{-1}, the velocity is greatly adjusted towards the target profile above $z = 400$ m but underestimates the target profile beneath $z = 200$ m. In the rotor area a good accordance between the nudged profile and the observed target profile can be seen for $f_0 = 0.0007$ s^{-1} where the difference between the curves is within the uncertainty range of the measurements.

Considering the meridional velocity $\langle v \rangle_{xy}$ (averaged over $x = 1200$ m ... 1800 m) the target profile is reached accurately in the rotor area for $f_0 = 0.0007$ s^{-1}, $f_0 = 0.001$ s^{-1}, and $f_0 = 0.0015$ s^{-1}, respectively. Between z = 250 m and $z = 400$ m the assimilation method was able to adjust the meridional velocity notably for $f_0 = 0.0015$ s^{-1}. Above z = 400 m the best results are achieved for $f_0 = 0.001$ s^{-1} and $f_0 = 0.0015$ s^{-1}.

Regarding the TKE, a small reduction of the atmospheric turbulence can be seen for $f_0 = 0.0005$ s^{-1} while larger frequencies lead to an increase of the TKE between z = 50 m and z = 280 m. In this area the TKE values for $f_0 = 0.0007$ s^{-1}, $f_0 = 0.001$ s^{-1} and 0.0015 s^{-1} are in between the values of the precursor simulation and the measured TKE. Compared to the measurements inside the rotor area the TKE for $f_0 = 0.001$ s^{-1} leads to the closest values within the uncertainty range of ± 0.2 m^2 s^{-2} of the measurement data.

It can be concluded that the best results can be obtained when the frequency in the vibration assimilation method is set to $f_0 = 0.0007$ s^{-1}, as the zonal target profile is matched more precisely than in the other cases, especially in the area of the rotor, whereas the meridional velocity is within the uncertainty range for all tested frequencies. Furthermore, inside the rotor area the calculated TKE for this f_0 is in between the precursor simulation and the measured TKE. For the following simulations with the wind turbines we give a precise math of the zonal and meridional wind components a higher priority than TKE. Therefore, synchronized two-dimensional slices are extracted at x = 1500 m from the nudging simulation with $f_0 = 0.0007$ s^{-1}, serving as turbulent inflow.

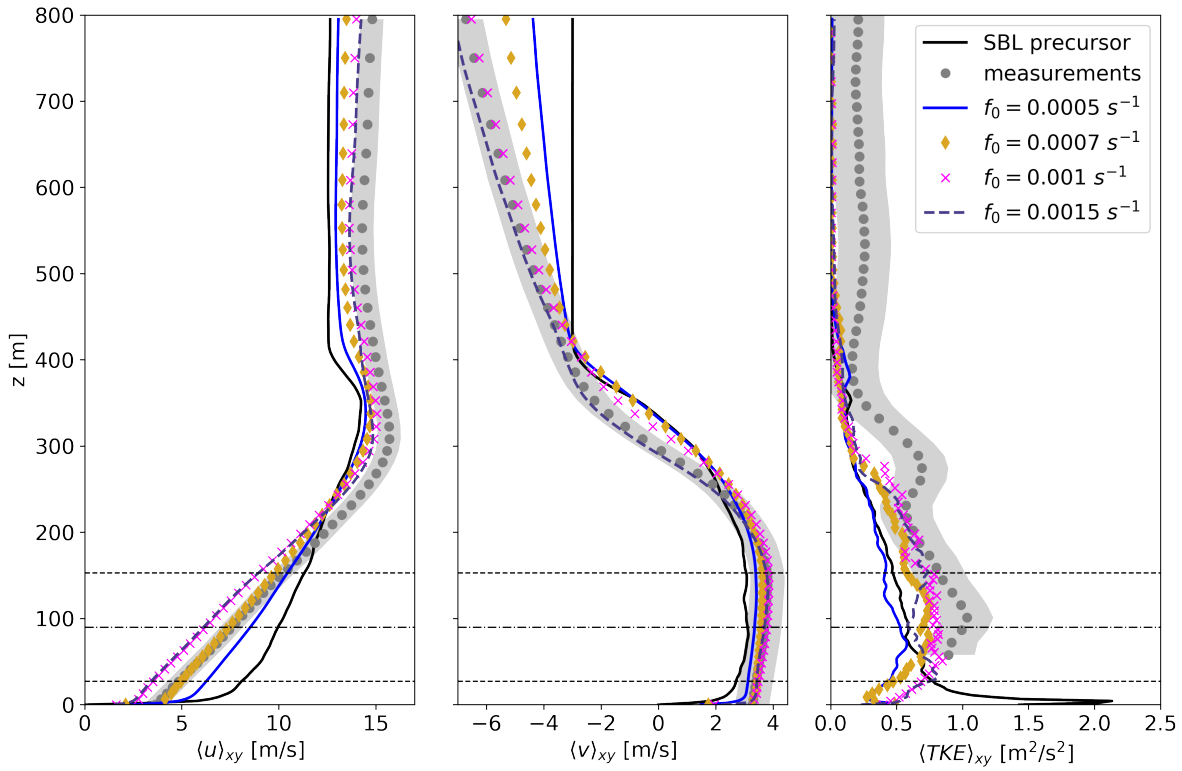

Figure 2. Results of the vibration assimilation method using different frequencies f_0 for the calculation of the additional forcing. The mean zonal velocity $\langle u \rangle_{xy}$, the mean meridional velocity $\langle v \rangle_{xy}$ and the mean TKE is presented, horizontally averaged at each vertical level. The black solid line refers to the values of the precursor simulation while the gray dotted line shows the measured target profiles for $\langle u \rangle_{xy}$ and $\langle v \rangle_{xy}$ and the measured TKE. The uncertainty of the measurements ± 0.6 m s^{-1} (± 0.2 m^2 s^2) for the velocities (TKE) is indicated by the gray colored area. The horizontal thin dashed (dashed dotted) lines show the top tip and bottom tip (center) of the rotor. The blue line (gold diamonds, magenta crosses, dark blue dashed line) shows the resulting profiles for a frequency of $f_0 = 0.0005$ s^{-1} ($f_0 = 0.0007$ s^{-1}, $f_0 = 0.001$ s^{-1}, $f_0 = 0.0015$ s^{-1}).

3.3. Mean profiles interacting with a wind-turbine rotor

Figure 3 shows the distribution of the temperature profile, the mean streamwise and spanwise velocity and the mean TKE up to $z = 200$ m. Compared are the values for the measurements, the precursor SBL and the nudging simulation with $f_0 = 0.0007$ s^{-1}. The streamwise and spanwise velocities are in very good agreement with the measured profiles as well as the mean TKE inside the rotor area. The left image shows the temperature profile, which is not affected by the assimilation approach. It can be concluded that the assimilation of the wind profiles leads to an SBL with realistic wind speeds and turbulence especially inside the rotor area. Before the turbulent flow from the assimilation simulation can be applied as inflow condition in the wind-turbine simulation, the flow field is rotated to result in a spanwise velocity of zero at turbine hub height. The resulting flow field allows the further simulation of the two wind turbines in a row with this assimilated inflow and the investigation of the developed wake.

3.4. Wind-farm simulation

The presented approach shows a successful adaption of the mean profiles of the zonal and meridional wind components towards the measurements, while TKE is only affected in response

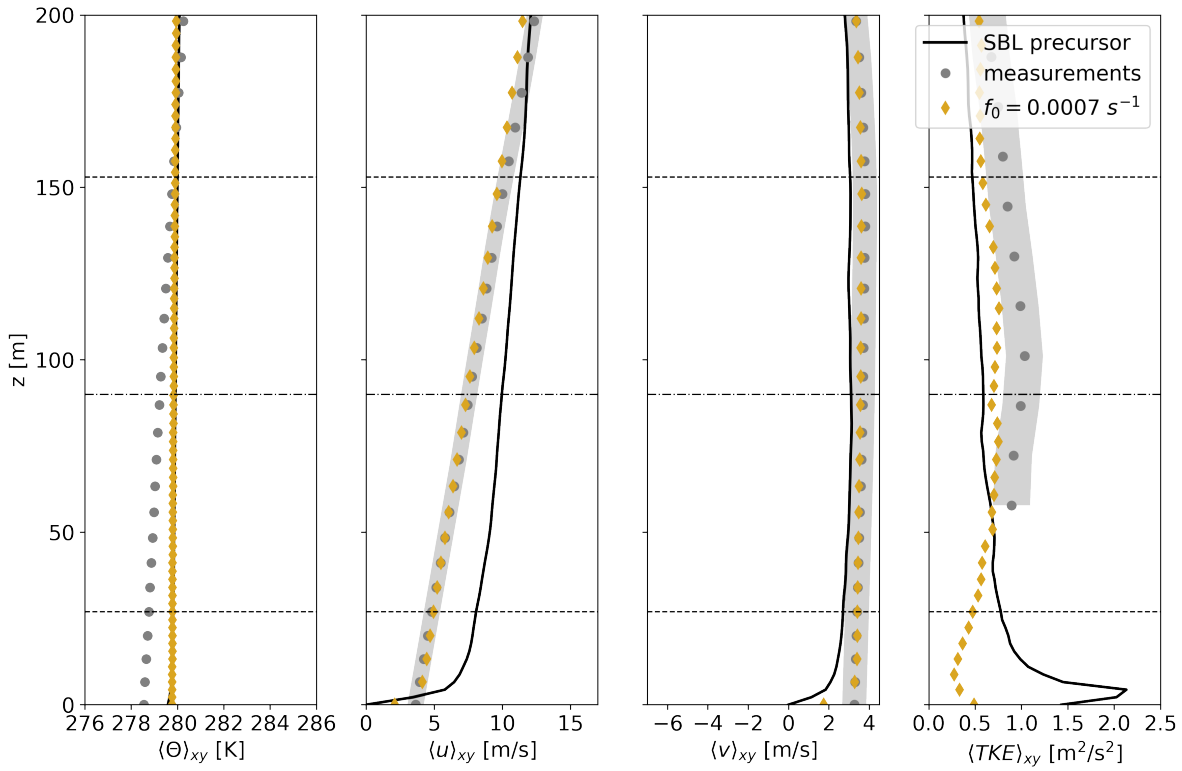

Figure 3. Vertical mean profiles of the potential temperature $\langle\Theta\rangle_{xy}$, the wind components $\langle u\rangle_{xy}$, $\langle v\rangle_{xy}$ and $\langle TKE\rangle_{xy}$ (resolved + subgrid scale) obtained from different sources. The gray points show the measured target profiles from the Krummendeich research windfarm with the measurement uncertainties (cf. Fig. 2) indicated by the colored areas. The black solid line indicates the profile from the idealized precursor simulation. The gold diamond line indicates the final profile obtained from the vibration assimilation method. The horizontal thin dashed (dashed dotted) lines show the top tip and bottom tip (center) of the rotor.

to the shear production by the adjusted flow (Eq. 2). The final aim of this approach will be a suitable method to adapt the mean flow conditions from an idealized LES towards measurements, which can be used as inflow conditions for wind-turbine simulations. As first attempt, we perform wind-turbine simulations following Sect. 2.5. As no wind turbines and, therefore, no wake measurements were available at Krummendeich in 2021, this presents a general test of the proposed simulation chain, giving a first impression of the wake including the assimilation technique.

Figure 4 shows x-y cross sections through hub height on the left and x-z cross sections through the center of the nacelle on the right. The first row represents the resulting wakes under idealized inflow conditions of the SBL and the second row the corresponding wakes under nudged inflow conditions. The main difference is the modified wind field interacting with the upwind rotor. The streamwise wind component of the idealized SBL is reduced by the assimilation approach towards the measurements. The different hub height wind speed (Fig. 3) correspond to a difference in the rotor speed for the 5 MW NREL rotor. Therefore, the wind turbine simulated with inflow data from the precursor simulation is in a different operating point in comparison to the wind turbine simulated with inflow data from the assimilation simulation.

However, apart from differences in the absolute velocity values, resulting from a smaller inflow velocity and related differences in the rotor performance, the general wake structures are similar.

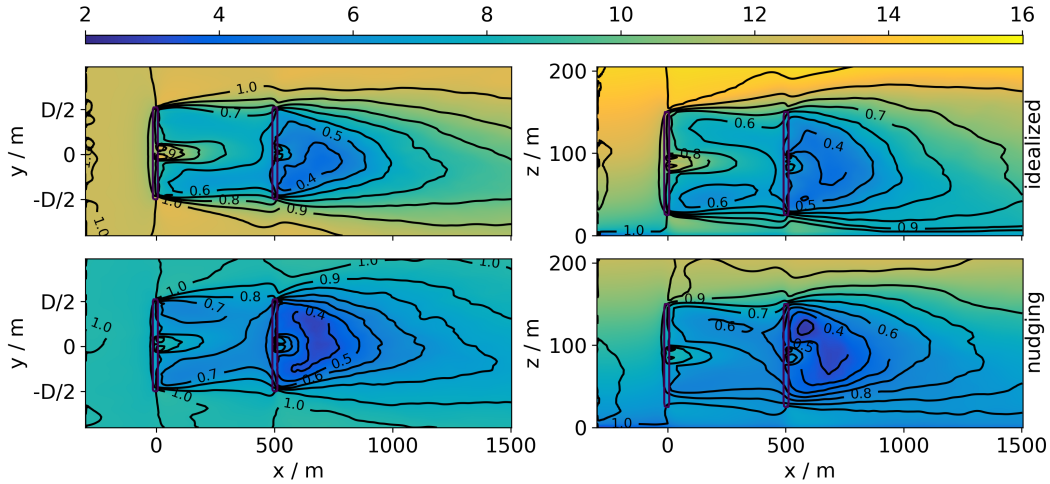

Figure 4. Coloured contours of the streamwise velocity component in m s^{-1} as horizontal cross section $\overline{u_{i,j,k_{hub}}}$ through hub height k_{hub} (left) and as vertical cross section $\overline{u_{i,j_0,k}}$ through the center of the rotor j_0 (right). The idealized inflow is presented in the top row and the nudged inflow towards measurements in the bottom row. All are averaged over the last 10 min of the corresponding wind-turbine simulation. The black contours represent the velocity deficit $VD_{i,j,k_{hub}}$ (left) and $VD_{i,j_0,k}$ (right).

The minimum of the velocity deficit ($VD_{i,j,k} \equiv \frac{\overline{u_{1,j,k}} - \overline{u_{i,j,k}}}{\overline{u_{1,j,k}}}$, black contours in Fig. 4) of 0.6 to 0.7 is prevalent after the first rotor in both cases. Likewise it is the case with the near-wake VD-value of ≈0.4 behind the downwind rotor. The downstream distance of the corresponding VD-lines is comparable, with a slightly more rapid wake recovery in the assimilated wind-farm simulation. This intensified entrainment can be explained with the influence of the forcing from the assimilation process on the velocity field in Eq. 3, resulting in an increase of TKE (Figs. 2 and 3) in the inflow wind field of the nudged wind-farm simulation. Despite the different rotor speed in the two wind-farm simulations, the general wake characteristics (wake width, wake extension, VD) are preserved by the assimilation approach. For a final validation, a comparison with measurements will be necessary in the future.

4. Conclusion

A simulation chain consisting of three components is necessary to represent the wake of a wind park in stably-stratified ABL flow for a prescribed vertical mean profile of the horizontal wind. The high-resolved precursor simulation with an SGS model which is capable to account for the pertinent atmospheric turbulence in the SBL provides a simulation which matches to a large extend previously defined parameters of observational data. However, there are still differences between the simulated and the measured horizontal velocities and TKE, which are most likely due to mesoscale atmospheric processes that are present in the observations but not taken into account in the numerical simulations. The mesoscale impact on the same stably-stratified situation is investigated in detail in Kilroy et al. [21] by simulations with WRF leading to results of windspeeds and TKE values in accordance with the measurements.

The presented vibration assimilation technique is able to nudge the velocities towards the desired target profiles. Especially, the measured velocity profiles are represented accurately in the area of the wind-turbine rotor. The impact of the assimilation technique on the TKE has been presented. Instead of a damping of the TKE, which occurs using a Newtonian relaxation (cf. [18]), the assimilation technique applying the vibration equation leads to an increase of the

TKE in comparison to the idealized precursor simulation. As the results within the rotor area are very convincing, the flow through the wind farm is simulated as the third component of the applied simulation chain.

This study is a first approach towards a wind-turbine simulation under realistic turbulent inflow conditions. Our next step is not only to adjust the mean wind profiles, but also to take turbulence into account so that its effect leads to the final mean wind profiles. Another step would be the adaption of the potential temperature profile towards measurements. As soon as measurement data of the wakes will be available for the wind farm WiValdi at Krummendeich, a detailed comparative analysis between measurements and simulations will be performed which will improve knowledge of the interaction of wakes with realistic atmospheric flow.

Acknowledgements

The authors gratefully acknowledge the Gauss Centre for Supercomputing e.V. (https://www.gauss-centre.eu) for funding this project by providing computing time on the GCS Supercomputer SuperMUC at Leibniz Supercomputing Centre (LRZ, https://www.lrz.de).

References

[1] Stull, R. B. 1988 An Introduction to Boundary Layer Meteorology *Kluwer Academic*
[2] Maronga, B., and Li, D. 2022 An investigation of the grid sensitivity in large-eddy simulations of the stable boundary layer. *Boundary-Layer Meteorology* **182(2)**
[3] Beare, R. J. et al. 2006 An intercomparison of large-eddy simulations of the stable boundary layer *Boundary-Layer Meteorology* **118**
[4] Schumann, U. 1991 Subgrid length-scales for large-eddy simulation of stratified turbulence *Theoretical and Computational Fluid Dynamics* **2(5-6)**
[5] Sullivan, P. P., McWilliams, J. C., and Moeng, C. H. 1994 A subgrid-scale model for large-eddy simulation of planetary boundary-layer flows. *Boundary-Layer Meteorology* **71**
[6] Kosović, B. and Curry, J. A. 2000 A large eddy simulation study of a quasi-steady, stably stratified atmospheric boundary layer *J atmos sci* **57(8)**
[7] Sullivan, P. P., Weil, J. C., Patton, E. G., Jonker, H. J., and Mironov, D. V. 2016 Turbulent winds and temperature fronts in large-eddy simulations of the stable atmospheric boundary layer *J atmos sci* **73(4)**
[8] Allaerts, D., Quon, E., Draxl, C., and Churchfield, M. 2020 Development of a time-height profile assimilation technique for large-eddy simulation. *Boundary-Layer Meteorology* **176(3)**
[9] Nakayama, H. and Takemi, T. 2020 Development of a Data Assimilation Method Using Vibration Equation for Large-Eddy Simulations of Turbulent Boundary Layer Flows. *J adv model earth sy* **12(8)**
[10] Allaerts, D., Quon, E., and Churchfield, M. 2023 Using observational mean-flow data to drive large-eddy simulations of a diurnal cycle at the SWiFT site. *Wind Energy* **26(5)**
[11] Wildmann, N., Hagen, M., and Gerz, T. 2022 Enhanced resource assessment and atmospheric monitoring of the research wind farm WiValdi. *J. Phys. Conf. Ser.* **2265(2)**
[12] Prusa, J. M., Smolarkiewicz, P. K., and Wyszogrodzki, A. A. 2008 EULAG, a computational model for multiscale flows *Comput. Fluids* **37**
[13] https://windenergy-researchfarm.com
[14] Chamorro, L. P. and Porté-Agel F. 2010 Effects of thermal stability and incoming boundary-layer flow characteristics on wind-turbine wakes: a wind-tunnel study. *Boundary-Layer Meteorology* **136(3)**
[15] Stoll, R., Gibbs, J. A., Salesky, S. T., Anderson, W., and Calaf, M. 2020 Large-Eddy Simulation of the Atmospheric Boundary Layer *Boundary-Layer Meteorology* **177**
[16] Maronga, B. et al. 2015 The Parallelized Large-Eddy Simulation Model (PALM) version 4.0 for atmospheric and oceanic flows: model formulation, recent developments, and future perspectives. *Geoscientific Model Development* **2515(8)**
[17] Stauffer, D. R. and Seaman, N. L. 1990 Use of four-dimensional data assimilation in a limited-area mesoscale model. Part I: Experiments with synoptic-scale data. *Monthly Weather Review* **118(6)**
[18] Wrba, L., Englberger, A., Dörnbrack, A., Kilroy, G. and Wildmann, N. 2024 Data assimilation of realistic boundary-layer flows for wind-turbine applications - An LES study *Wind Energy Science Discussions*
[19] Englberger, A. and Dörnbrack, A. 2018 Impact of the diurnal cycle of the atmospheric boundary layer on wind-turbine wakes: A numerical modelling study *Boundary-Layer Meteorology* **166**
[20] Wildmann, N., Päschke, E., Roiger, A., and Mallaun, C. 2020 Towards improved turbulence estimation with Doppler wind lidar velocity-azimuth display (VAD) scans *Atmospheric Measurement Techniques* **4141–4158**
[21] Kilroy, G., Englberger, A., Wrba, L., Bührend, L., and Wildmann, N. 2024 Evaluation of turbulence characteristics in WRF simulations at WiValdi wind park *J. Phys. Conf. Ser. (under review)*